

Block Polymer Micelles Enable CRISPR/Cas9 Ribonucleoprotein Delivery: Physicochemical Properties Affect Packaging Mechanisms and Gene Editing Efficiency

Zhe Tan,[†] Yaming Jiang,^{‡,#} Mitra S. Ganewatta,^{†,||} Ramya Kumar,[†] Allison Keith,[§] Kirk Twaroski,[§] Thomas Pengo,[§] Jakub Tolar,[§] Timothy P. Lodge,^{†,‡} and Theresa M. Reineke^{*,†}

[†]Department of Chemistry, University of Minnesota, Minneapolis, Minnesota 55455, United States

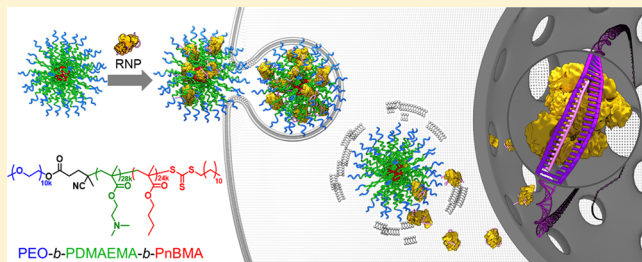
[‡]Department of Chemical Engineering and Materials Science, University of Minnesota, Minneapolis, Minnesota 55455, United States

[§]Department of Pediatrics, Stem Cell Institute, University of Minnesota Medical School, Minneapolis, Minnesota 55455, United States

^{*}University of Minnesota Informatics Institute, University Imaging Center, Minneapolis, Minnesota 55455, United States

S Supporting Information

ABSTRACT: Gene editing with CRISPR/Cas9 is revolutionizing biotechnology and medical research, yet affordable, efficient, and tailorabile delivery systems are urgently needed to advance translation. Herein, a series of monodisperse amphiphilic block polymers poly[ethylene oxide-*b*-2-(dimethylamino) ethyl methacrylate-*b*-*n*-butyl methacrylate] (PEO-*b*-PDMAEMA-*b*-PnBMA) that housed three PEO lengths (2, 5, and 10 kDa) and a variant lacking PEO (PDMAEMA-*b*-PnBMA) were synthesized via controlled radical polymerization and assembled into well-defined spherical cationic micelles. The cationic micelles were complexed via electrostatic interactions with Cas9 protein/guide RNA ribonucleoproteins (RNPs) that exhibit anionic charges due to the overhanging RNA. The resulting micelleplex formulations in both phosphate-buffered saline (PBS) and water were screened via high content analysis for gene editing efficiency. The micelle variant with the 10 kDa PEO block offered the highest gene editing performance and was advanced for in-depth characterization. For the first time, quantitative static and dynamic light scattering characterization and cryogenic transmission electron microscopy images of Cas9 protein/guideRNA RNP loading into well-defined micelleplex nanoparticles are revealed, where the formulation solvent was found to play a major role in the physicochemical properties and biological performance. In PBS, the solutions containing the micelles (63 triblock polymers per micelle) were assembled with the Cas9 protein/guideRNA RNP payloads offering uniform loading of 14 RNPs per micelleplex and moderate editing efficiency; this homogeneous system offers promise for future *in vivo*/preclinical applications. Interestingly, when the uniform micelles were formulated with the RNP payloads in water, larger multimicelleplex nanoparticles were formed that offered double the editing efficiency of Lipofectamine 2000 (40% gene editing) due to the rapid sedimentation kinetics of the larger colloids onto adherent cells, offering promising *in vitro*, *ex vivo*, and/or cell therapy applications. This work presents the first quantitative demonstration of tailorabile block polymer micelle formulations for advancing CRISPR/Cas9 RNP delivery and fundamental correlation of the solutions physics to biological performance.



INTRODUCTION

CRISPR (clustered regularly interspaced short palindromic repeats)/Cas9 (CRISPR-associated protein 9)-based genome editing has rapidly emerged as a multifaceted technology to enable gene insertion, deletion, activation, suppression, and even single base editing of target genes within the nucleus of any cell. This highly efficient and facile technique has broad utility from white biotechnology and agriculture to biomedical research, pharmaceuticals, and regenerative medicine.^{1,2} Various CRISPR systems continue to be rapidly evolved,^{3–5} and developing effective delivery systems is essential to the success

of this technology. Currently, the CRISPR/Cas9 system can be delivered *in vitro*, *ex vivo*, and *in vivo* in three different payload forms: (i) plasmid DNA (pDNA), which encodes Cas9 protein and/or single guide RNA (sgRNA) or (ii) mRNA that encodes for Cas9 nuclease and a separate sgRNA, or (iii) a ribonucleoprotein (RNP) that consists of recombinant Cas9 protein precomplexed directly with a sgRNA. While

Received: August 5, 2019

Revised: September 20, 2019

Published: October 21, 2019

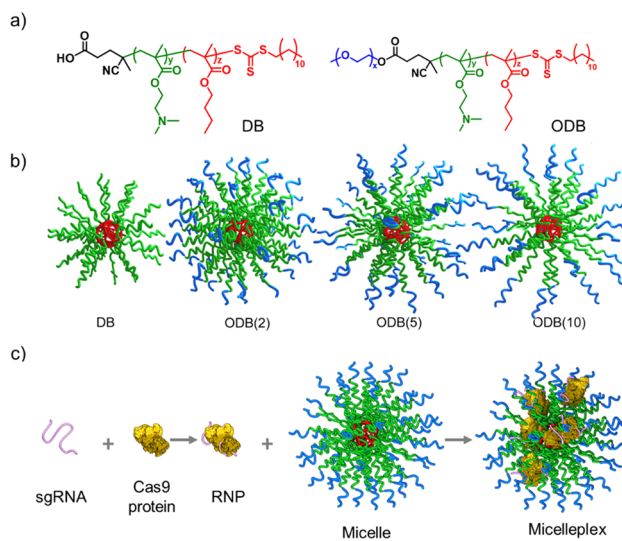
engineered viruses have shown exceptional delivery efficiency and expression of Cas9 protein in cells, limitations such as immunogenicity and size restrictions in packaging exist.^{6,7} Physical delivery methods such as electroporation and microinjection are known to cause cell damage or death and challenging to apply to a large population of cells/tissues.^{8–12}

Synthetic polymers have been widely studied as pDNA delivery vehicles due to their versatility, low toxicity, and the ability to encapsulate large pDNA payloads. Some recent examples indicate that synthetic polymer-based systems achieved pDNA-based gene editing both in vitro and in vivo.^{13–18} However, pDNA must enter the cellular nucleus to express, and consistent expression produces an overabundance of Cas9 protein. This can lead to increased off-target editing and mutagenesis, and thus, dangerous long-term side effects.^{19,20} Researchers have turned to deliver the CRISPR/Cas9 system in mRNA form to circumvent the barrier of nuclear entry, which has been recently reported with polymer-based nanoparticles.²¹ However, sgRNA often needs to be delivered separately, presenting challenges in the trafficking kinetics of different payloads.

Direct delivery of CRISPR/Cas9 ribonucleoprotein (RNP), on the other hand, has several benefits including precision in endonuclease dosing and potential to avoid uncontrolled integration of the transgene into the cellular genome. While different CRISPR/Cas9 RNP delivery systems have been recently explored, such as lipid-based nanoparticles,^{22–24} gold nanoparticles,^{25–27} cell-penetrating peptides,^{28–30} and other hybrid nanostructures,^{31–34} the mechanisms of payload encapsulation and the resultant complexes are generally not quantitatively understood/characterized. Polymers offer a well-documented pharmaceutically relevant platform that have been underexplored for RNP encapsulation and delivery, and only a limited number of reports have been presented,^{35–37} likely due to the inherent structural, charge, and binding differences of plasmid and protein-based payloads. Kang et al. reported a Cas9 protein covalently modified by branched polyethyleneimine and complexed with sgRNA to form nanocomplexes, which were shown to edit antibody-resistant bacteria.³⁷ Nevertheless, the requirement of the covalent modification of Cas9 protein makes the delivery vehicle less versatile to be applied for a variety of CRISPR variants. Wang et al. designed a poly(*N,N'*-bis(acryloyl)cystamine-*co*-triethylenetetramine)-based delivery system that encapsulated a variety of payloads including CRISPR/Cas9 RNP and achieved genome-editing efficiency similar to Lipofectamine 2000.³⁶ However, the complexes formed with the RNP payload were not well characterized or defined. To this end, designing novel and efficient polymer-based RNP delivery vehicles, as well as improving the fundamental understanding of polymer-RNP complex composition and architecture on protein loading and gene-editing efficiency, are necessary for advanced application.

Herein, we hypothesized that self-assembled cationic block polymer micelles can serve as a well-defined host to bind RNPs through electrostatic interactions with the sgRNA, enable quantitative characterization of packaging, and facilitate intracellular delivery and effective genome editing. To test this hypothesis, four polymer variants were created as shown in Scheme 1: a diblock copolymer was synthesized containing a poly(*n*-butyl methacrylate) (PnBMA) hydrophobic block (micelle core) and a cationic block consisting of poly(2-(dimethylamino)ethyl methacrylate) (PDMAEMA) (which forms the cationic brush corona on the micelle surface) that

Scheme 1. Schematic Illustrations of DB, ODB, and Micelle Structures and Micelleplex Formation^a



^a(a) diblock and triblock polymer structures, (b) micelle structures, and (c) micelleplex formulation and formation scheme with RNP payloads.

facilitates RNP binding and encapsulation, and three triblock terpolymer variants with systematically increasing poly(ethylene oxide) (PEO) block lengths (2, 5, and 10 kDa) to display nonionic hydrophilic PEO corona on the micelle surface. The four cationic micelle variants enabled the examination of the absence, presence, and length of PEO on RNP binding and biological properties. High-throughput dynamic light scattering (DLS) and high-content microscopy-based image cytometry methods were developed to assess the micelle-RNP complex (micelleplex) size and gene-editing efficiency, respectively, allowing selection of the top performer with the longest PEO length. Formulations of the optimal micelleplexes were then quantitatively characterized via a battery of techniques. It was discovered that micelleplexes can achieve up to 40% in vitro gene editing efficiency with engineered HEK 293T (human embryonic kidney) cells (twice the value observed with the positive control, Lipofectamine 2000). To the best of our knowledge, this is the first example of a polymer micelle system that successfully hosts CRISPR/Cas9 RNPs, quantitative characterization of RNP packaging, and correlation of formulation solution physics to the biological performance. This delivery system, along with the screening/structure selection workflow and quantitative characterization methods, have the potential to enable discovery and optimization of well-defined nonviral delivery vehicles for protein-based gene editing tools.

RESULTS AND DISCUSSION

Complex Formation. The PDMAEMA-*b*-PnBMA (DB) diblock copolymer and three PEO-*b*-PDMAEMA-*b*-PnBMA (ODB) triblock polymers were synthesized via reversible addition-fragmentation chain transfer (RAFT) polymerization to acquire uniform chain lengths. The polymers were characterized according to published procedures (Table 1).³⁸ The DB and ODB polymers self-assembled to form spherical micelles exhibiting core–shell or core–shell–corona architectures, respectively (Scheme 1). The PnBMA hydrophobic chain length was chosen such that after micelle formation, the

Table 1. Synthetic Block Polymer Characterization

parameters	polymer			
	DB	ODB(2)	ODB(5)	ODB(10)
block length (kDa)				
PEO		2	5	10
PDMAEMA	27	27	27	28
PnBMA	14	24	25	24
D	1.10 ^a	1.12 ^b	1.18 ^b	1.14 ^b

^aPreviously characterized by Sprouse et al.⁴¹ Measured by MALDI-TOF-MS. ^bPreviously characterized by Jiang et al.³⁸ measured by SEC-LS.

cores are kinetically constrained from chain exchange at room temperature due to the strong hydrophobic nature of PnBMA and long block length.^{39,40} Thus, micelles are stable with respect to size and shape.

The Cas9 protein used in this work was sNLS-spCas9-sNLS, which contains nuclear localization signals on both ends of the protein to promote efficient nuclear trafficking once delivered inside the cell. When forming micelleplexes, sgRNA was first added to Cas9 protein at a 1:1 molar ratio and allowed to complex for 15 min. Micelle solutions were then added to the RNP solution and allowed to further complex for 1 hr. The systems were examined at a polymer:RNP molar formulation ratio of both 2.5:1 and 5:1. All four micelle variants were designed to contain the same cationic (PDMAEMA) block chemistry and lengths, thus, at a certain polymer:RNP molar ratio, the molar ratio of RNP to amine groups are consistent across all four micelleplex formulations.

Micelleplex Formulation and High-Content Screening. Micelleplexes were formulated in two common solvents for biological delivery studies, phosphate buffer saline (PBS) and water, and characterized for size via high-throughput DLS (Figure 1). The four bare micelle species without RNP were found to have similar hydrodynamic radii (R_h), between 28–34 nm in PBS and slightly larger sizes of 30–44 nm in water, presumably due to the elongated cationic corona under low ionic strength, in agreement with the previous work on polycation solution physics.^{41,42} While the PEO block indeed adds some hydrodynamic volume, the PEO length did not appear to influence the hydrodynamic radius of the micelles under these conditions, as the aggregation number of the micelles decreases with increasing corona chain length.³⁸ All micelleplex formulations were found to have similar sizes in each respective solution after formulation regardless of micelle architecture. Micelleplexes formulated in PBS had R_h values around 30 nm, (similar to the bare micelles), indicating that the RNPs might nestle into the cationic block. In comparison, larger particles with R_h of around 135–155 nm were formed in water. To further understand the mechanistic phenomena associated with these differences, these results were examined in detail (vide infra).

An engineered HEK 293T cell line with an imbedded traffic light reporter (TLR) system was utilized as the model cell line to screen delivery efficiency and genome-editing.⁴³ The 20 bp sgRNA has been designed to target binding of the Cas9 nuclease to a genomic region upstream of an out-of-frame mCherry gene engineered into the HEK 293T genome. If the RNP is successfully delivered to the nucleus (and binds this genomic site), a double-strand DNA break (DSB) will occur at the target locus and then be repaired via nonhomologous end-joining (NHEJ), a native cellular mechanism that quickly

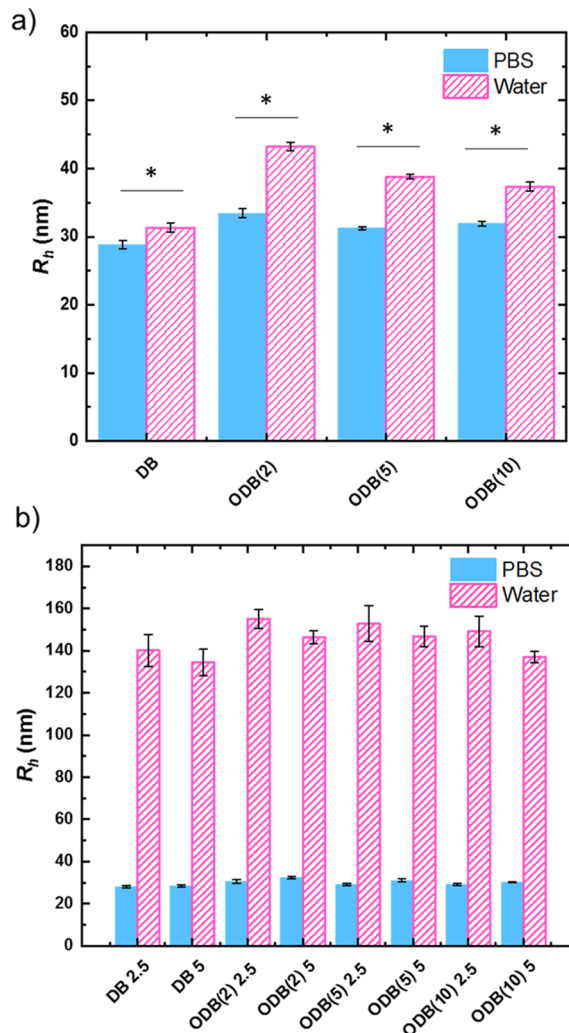


Figure 1. Micelle and micelleplex sizes formulated in water and PBS as measured by high-throughput DLS. Each sample was measured with 5 acquisitions ($n = 5$), 5 s each, with data representing mean \pm standard deviation. (a) Micelles only, (b) micelleplexes at a polymer:RNP molar ratio of 2.5:1 (denoted as 2.5) or 5:1 (denoted as 5). The asterisks “*” indicate statistically different ($p < 0.05$) analyzed by one-way ANOVA followed by a post hoc Tukey test.

ligates the broken ends through insertion or deletion (indel) base mutations. The indels cause frame shifts to occur in the downstream mCherry gene; a fraction of those indels lead to the correct frame shift to upregulate mCherry expression (red fluorescence), which can be visualized and quantified under fluorescence microscopy. It should be noted that the percentage of mCherry-positive (mCherry⁺) cells is lower than the percentage of total edited cells because not all frame shifts induce mCherry production. Nonetheless, this is a facile method for high content screening to speedily and efficiently identify the candidates that displayed the best editing outcomes, as measured by mCherry expression.

Using this cell line, we compared the gene-editing performance of different micelleplex formulations across 2 solvent environments (PBS and water), 4 micelle compositions, and 2 molar ratios, giving rise to 16 possible candidates. All of the micelleplex formulations were diluted with Opti-MEM (reduced serum media) immediately before transfection. The ionic strength (IS) of the micelleplex/water formulation would increase after media addition. Thus, to test whether the

IS increase during transfection affects micelleplex size in the water formulation, the solution was diluted with twice the volume of PBS (final solution IS = 103 mM), and a DLS measurement was performed. The results showed that after PBS dilution, micelleplexes have a slightly increased mean R_h of 215 nm ($\mu_2/\Gamma^2 = 0.30$). For the micelleplex/PBS formulation, media addition has a minimal effect on the solution IS, thus the particle characteristics were assumed to be unchanged. Forty-eight hours after transfection of the HEK 293T TLR cells with the micelleplex formulations and controls, the cell nuclei were stained with Hoechst and microscopy acquisition was performed. Finally, an image analysis pipeline developed in CellProfiler was used to compute the ratio of mCherry⁺ cells to the total number of nuclei in every image (further details are available in the Supporting Information). As shown in Figure 2 and Figure S1, in general, all micelleplex

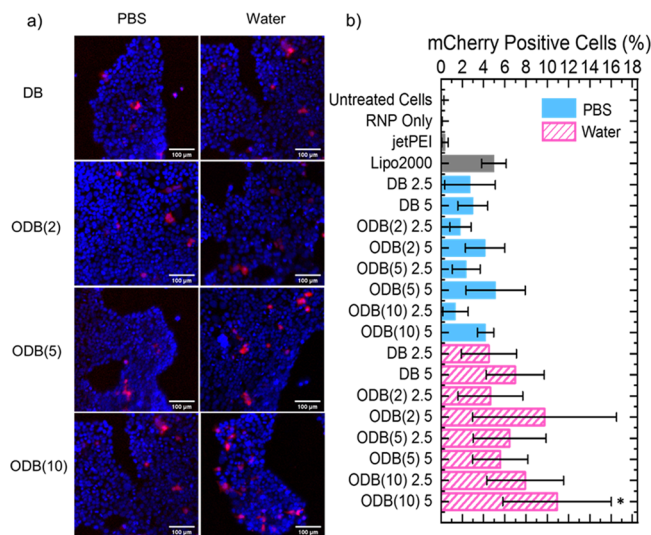


Figure 2. Gene-editing efficiency, indicated by mCherry expression level, in the engineered HEK-293T TLR cells was measured by high-content microscopy-based image cytometry. Micelleplexes were formed at Cas9:sgRNA:polymer molar ratio of 1:1:2.5. (a) Representative microscopy images. Blue dots are Hoechst-stained cell nuclei; red dots denote mCherry⁺ nuclei. Each transfection formulation was completed in duplicate, 4–15 images were taken per well, and the collective data were processed via a high content image analysis. Representative images at Cas9:sgRNA:polymer molar ratio of 1:1:5 can be found in the Supporting Information (Figure S1). (b) Summarized results of % mCherry⁺ cells. Data are presented as mean of % mCherry⁺ cells in each image \pm standard deviation. The asterisk “*” indicates statistically higher compared to Lipofectamine 2000 ($p < 0.05$). Data were analyzed by one-way ANOVA followed by a post hoc Tukey test.

formulations promoted mCherry expression higher than the jetPEI control, and many formulations appeared to match the efficiency promoted by Lipofectamine 2000 (5% mCherry⁺) or even higher levels (av 2–11% mCherry⁺). Since high mCherry expression is indicative of high editing efficiency, it was concluded that the formulations in water reached higher editing efficiencies (av 5–11% mCherry⁺) than formulations in PBS (av 2–5% mCherry⁺). We suggest that higher delivery efficiency in water is potentially a consequence of the larger complex size and higher settling velocities, which is further discussed below. Moreover, all micelleplexes formed in water exhibited similar or higher editing efficiency compared to

Lipofectamine 2000, regardless of the micelle architecture. Using this process, the ODB(10) variant, which promoted statistically higher mCherry expression than Lipofectamine, was identified as the best candidate vehicle and the focus of extensive biophysical characterization.

Quantitative Characterization of ODB(10) Micelleplexes. Micelleplex complexation was characterized by gel electrophoresis (Figure 3a). In both PBS and water, sgRNA migrates toward the anode due to its overall negative charge. After complexation with Cas9 protein, the RNP migration in PBS was less than that of sgRNA, indicating stable binding of the sgRNA to the Cas9 protein, which maintained an overall negative charge. However, in water, the RNP migration was completely impeded, which potentially denoted the formation of large RNP aggregates. Upon addition of micelles, the complete lack of RNP migration in both PBS and water suggested the formation of micelleplexes. Zeta potential analysis (Figure 3b) showed that overall, particles had higher absolute values of Zeta potential in water compared to PBS, due to low solution ionic strength. In both solvent conditions, the RNP sample exhibited a negative Zeta potential due to the overhanging negative charge on the sgRNA, which leads to electrostatic interaction with the cationic micelle brush. As expected, the Zeta potential of the micelles was highly positive and decreased slightly after micelleplex formation.

To quantitatively analyze and compare the size, composition, morphology, and RNP loading of the ODB(10) micelleplexes in PBS and water, multiangle DLS and cryo-TEM characterizations were performed. The DLS results revealed that in PBS, RNP has a hydrodynamic radius (R_h) of around 9 nm (Figure 3c), which is in agreement with the single RNP size in a previous report.⁴⁴ The micelleplexes formed in PBS have R_h values of 26 nm ($\mu_2/\Gamma^2 = 0.13$) and 27 nm ($\mu_2/\Gamma^2 = 0.06$) at ODB(10) polymer:RNP molar ratio 2.5:1 and 5:1, respectively, slightly smaller than the uncomplexed micelles (Figure 3c and Table S1). This result provides evidence that the micelleplexes in PBS consist of single micelles, and that the binding between the PDMAEMA cationic midblock and RNP leads to a slight contraction of the micelle corona. This observation of micelle compaction is in agreement with previous literature showing that the complexation of oppositely charged polyelectrolytes leads to a micelle corona contraction.⁴⁵ By comparison, the RNPs have large particle sizes ($R_h > 500$ nm) in water (Figure 3d), presumably due to the collective aggregation of multiple RNPs under low ionic strength and/or electrostatic bridging of the cationic Cas9 protein with the anionic sgRNA. Interestingly, the formation of micelleplexes helped to reduce the degree of RNP aggregation by reducing the micelleplex R_h to around 150 nm. The above phenomena indicated different mechanisms of micelleplex formation under different buffering conditions. In PBS, the single micelles appear to act as the “template host” to RNPs for micelleplex formation, where individual RNPs bind within the ionic brush layer. In water, however, the RNPs may form loose aggregates, thus serving as the “template host” and micelles appear to break up the loose aggregates, that bind around the proteins and interact with RNPs to form larger multimicelle complexes. This could significantly influence particle settling kinetics (and thus cellular contact) in adherent cell transfection experiments.

The complexation mechanisms and the morphology of micelleplexes were further corroborated by cryogenic transmission electron microscopy (cryo-TEM) as displayed in Figures 4 and 5. The single micelles and RNPs were clearly

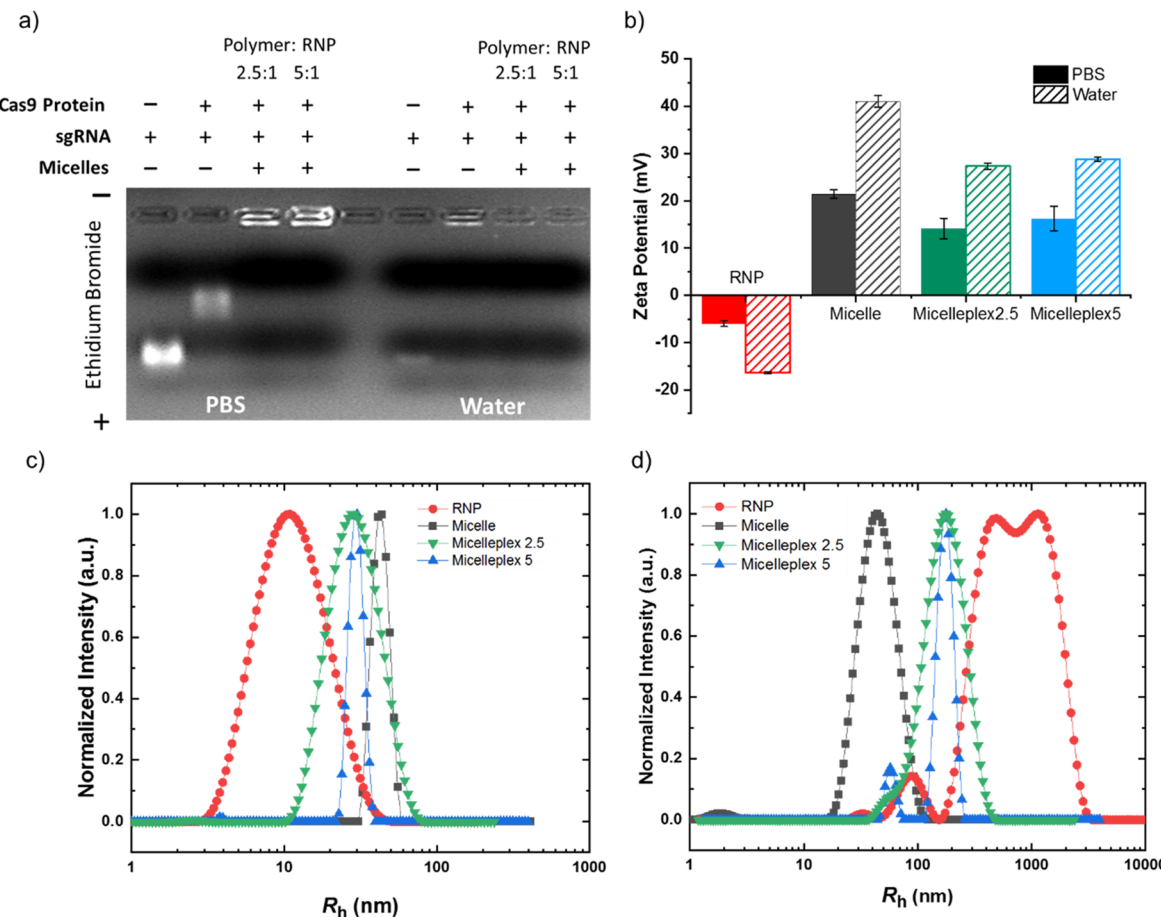


Figure 3. Characterization via gel shift, Zeta potential, and DLS. (a) Gel electrophoresis assay of sgRNA only, RNP, and micelleplexes at ODB(10) polymer:RNP molar ratio of 2.5:1 and 5:1, in both PBS and water conditions. (b) Zeta potential of RNP, micelles, and micelleplexes in PBS and water ($n = 3$). Data are shown as mean \pm standard deviation. (c, d) Hydrodynamic radii (R_h) of RNP, ODB(10) micelles, and their micelleplexes by (c) DLS in PBS and (d) in water. Size distributions were acquired by applying the REPES algorithm to the correlation function obtained at 90°.

imaged prior to complexation in PBS (Figure 4a,b). It is worth noting that while the micelle core is visible, the corona consisting of the solvated PDMAEMA and PEO blocks has a lower electron density and is not visualized due to the low contrast (Figure 4a). After micelleplex formation, the micelle corona has an increased contrast due to RNP binding and becomes visible (Figure 4c,d), and discrete RNPs can be visualized as higher contrast spots within the micelle corona. Due to RNP payload loading and increased contrast, the size of RNP-micelle complexes appears visually larger in the cryo-TEM compared to the micelles, even though in the DLS data, the overall hydrodynamic diameter actually contracts to promote complexation. Moreover, the micelleplexes in PBS appear to be spherical, and all micelleplexes contain single micelles, which is also in agreement with the previous DLS data. At ODB(10) polymer:RNP molar formulation ratio 2.5:1, some RNPs can be visualized in an uncomplexed free RNP state (Figure 4c), and the amount of free RNP is largely reduced at higher polymer formulation ratio (ODB(10) polymer:RNP 5:1), which is evidenced by the lack of free RNP in the cryo-TEM image in Figure 4d. In contrast, when the RNPs are diluted in water, they form large multiprotein aggregates of various sizes (Figure 5a and Figure S8). After formulation with the micelles, the micelleplexes clearly exhibit smaller sizes compared to RNP only (Figure 5b,c), which is in agreement with our previous data and hypothesis that

formation of micelleplexes help break up the larger aggregates of RNPs. This could also be the reason why the ODB(10) micelle with the longest PEO block performs better than the other micelle variants. The long PEO corona can potentially provide effective hydrophilic shielding and thus have better stabilization effect to the micelleplexes. In addition, free unbound micelles can also be visualized at both polymer:RNP ratios, which is opposite to the observation in PBS. These images provide further evidence of the different complexation mechanisms of micelleplex formation in PBS and water, which influences their biological performance.

Based on the DLS and cryo-TEM results, uniform micelles and micelleplexes are formed in PBS, thus enabling further quantitative analysis via static light scattering (SLS). Berry plots were used to extract the radius of gyration (R_g) and weight-averaged molar mass (M_w) of micelles and micelleplexes (Figures S2–S3). The ratio between R_g and R_h can provide the conformation and shape information of polymers and complexes. Bare micelles without RNPs exhibited an average R_g of 22 nm, and the R_h of micelles were measured to be 30 nm by DLS (Figure 3a and Table S1). Thus, the R_g/R_h value of the bare micelles was calculated to be 0.73, close to that of a hard sphere (0.78).⁴⁶ The M_w of micelles was measured to be 3.9×10^6 g/mol. With the assumption that all micelles are uniform and share the same composition, and given that each polymer chain has an M_w of 6.2×10^4 g/mol,

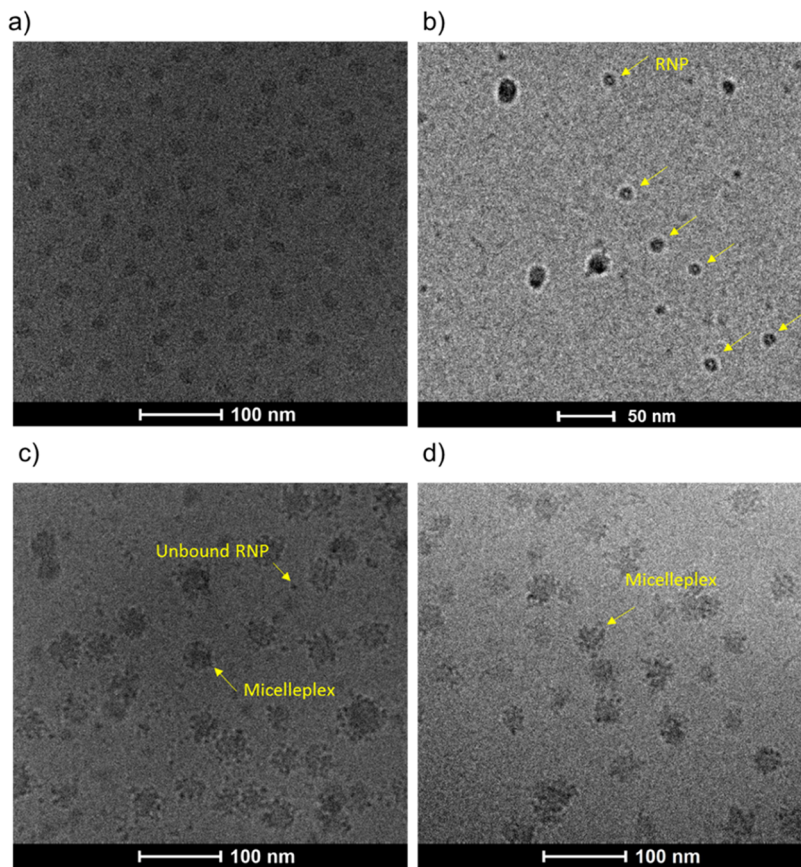


Figure 4. Representative cryo-TEM images in PBS of (a) ODB(10) micelles, (b) RNPs, (c) micelleplexes at ODB(10) polymer:RNP molar formulation ratio 2.5:1, and (d) micelleplexes at ODB(10) polymer:RNP molar formulation ratio 5:1. Additional supporting cryo-TEM images are displayed in Figures S4–S7, Supporting Information.

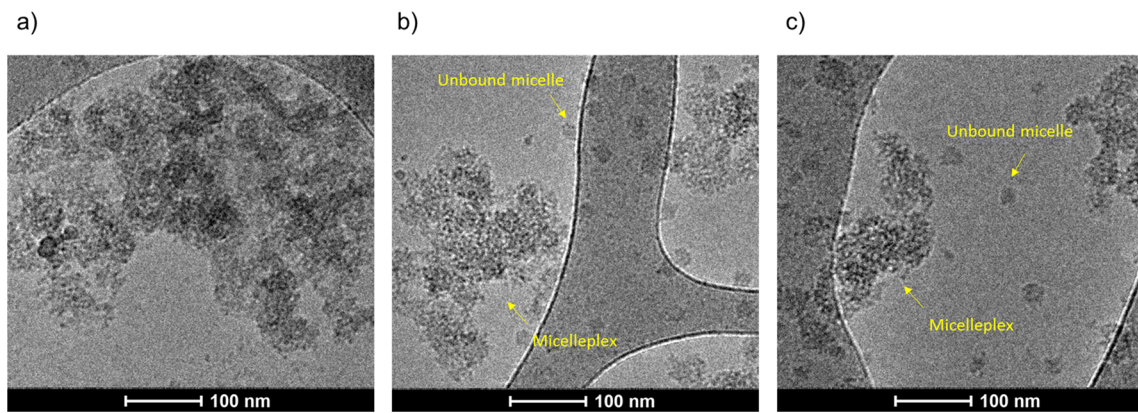


Figure 5. Representative cryo-TEM images in water of (a) RNPs, (b) micelleplexes at ODB(10) polymer:RNP molar formulation ratio 2.5:1, and (c) micelleplexes at ODB(10) polymer:RNP molar formulation ratio 5:1. Additional cryo-TEM images are available in Figures S8–S10, Supporting Information.

an average of 63 polymer chains are calculated to be present per ODB(10) micelle (micelle aggregation number $N_{\text{agg}} = 63$). Thus, when formulated with the RNPs at ODB(10) polymer:RNP molar ratios 2.5:1 and 5:1, the micelle:RNP molar formulation ratios are 1:25 and 1:13, respectively. Micelleplex composition and properties at polymer:RNP molar ratio of 2.5:1 were also characterized by SLS. This result indicated an R_g of 29 nm, larger than the R_g of micelle only, due to the increased weight and density on micelleplex corona after RNP binding. With the R_h of 26 nm by DLS, micelleplexes have a R_g/R_h value of around 1.1, closer to

that of a soft sphere (1.0).⁴⁶ The M_w of ODB(10)-RNP micelleplexes was calculated to be 5.2×10^6 g/mol. Under the assumption that every micelleplex contains the same number of RNPs and that all micelles were complexed, we calculate that each micelle housed on average 14 RNPs (calculation detailed in the Supporting Information). Thus, under polymer:RNP ratio 2.5:1, which is micelle:RNP molar ratio 1:25, around 56% of RNPs were bound to the micelles, indicating that some free RNP exists in the solution, which is in agreement with the cryo-TEM images where the free unbound RNPs can clearly be visualized (Figure 4c). In comparison, at a polymer:RNP molar

ratio 5:1, which is a micelle:RNP molar ratio of 1:13, the number of micelles is sufficient to house all the RNPs, thus there should be no free RNP in solution, which is also in agreement with the cryo-TEM results (Figure 4d). The quantitative properties of the micelles and micelleplex solutions are summarized in Table 2.

Table 2. Quantitative Characterization and Analysis of Micelles and Micelleplexes

properties	micelle	micelleplex ^a
M_w (g/mol) ^b	3.9×10^6	5.2×10^6
R_g (nm) ^b	22	29
R_g/R_h	0.73	1.1
A_2 ($\text{cm}^3 \text{ mol/g}^2$) ^b	2.3×10^{-5}	8×10^{-5}
N_{agg} ^c	63	
# amine/micelle ^d	11,000	
pKa of PDMAEMA block ²⁵	7.8	
percent amine protonated at pH = 7.4	73%	
# protonated amine/micelle	8,000	
micelle:RNP molar formulation ratio		1:25
micelle:RNP molar binding ratio ^e		1:14
# micelle/complex ^f		1
percent RNP bound		56%

^aAt 1:25 micelle:RNP molar formulation ratio. ^bData acquired by SLS. ^cMicelle aggregation number (N_{agg}) denotes the number of polymer chains per micelle. ^dNumber of amine groups per micelle (# amine/micelle) was calculated as a product of the number of 2-(dimethylamino) ethyl methacrylate (DMAEMA) repeat units per polymer chain and N_{agg} . ^eCalculated from SLS data (details are available in the Supporting Information). ^fClaimed based on DLS data, which showed similar particle size of micelle and micelleplexes.

Quantification of ODB(10) Micelleplex Gene-Editing Efficiency.

HEK 293T TLR cells were transfected with ODB(10) micelleplexes, and 48 h after transfection, the percent mCherry⁺ cells were measured quantitatively by flow cytometry. The results revealed that the micelleplexes formed in PBS produced around 2.2% mCherry⁺ cells for both RNP:micelle molar ratios, which is higher than the 1.0% produced with the jetPEI positive control, but lower than Lipofectamine 2000 (Figure 6a). Micelleplexes formed in water, however, offered 6.4–6.6% mCherry⁺ cells, which is higher than the 4.9% of mCherry⁺ cells with Lipofectamine 2000. These data showed a similar trend to the high content screens comparing the performance of ODB(10) micelles to the controls. As discussed previously, only a fraction of the indels generated by gene-editing lead to the correct frame shift to promote the expression of mCherry protein; thus, this assay is a significant underestimation of total gene editing in the cellular population.

To further quantify and compare the total gene-editing efficiency of the micelleplex formulations and controls, capillary Sanger sequencing was applied to the targeted genome locus of the HEK 293T TLR cell line for all transfected samples. A TIDE (Tracking of Indels by DEcomposition) computational assay⁴⁷ was then utilized to analyze the data. Briefly, the TIDE assay compares the wild-type untreated cell DNA sequence, acquired from standard Sanger sequencing, with the DNA sequence of edited samples, and generates the frequency of targeted mutations. At ODB(10) polymer:RNP molar ratios of 2.5:1 and 5:1, the micelleplexes in PBS showed a total gene editing of 4% and

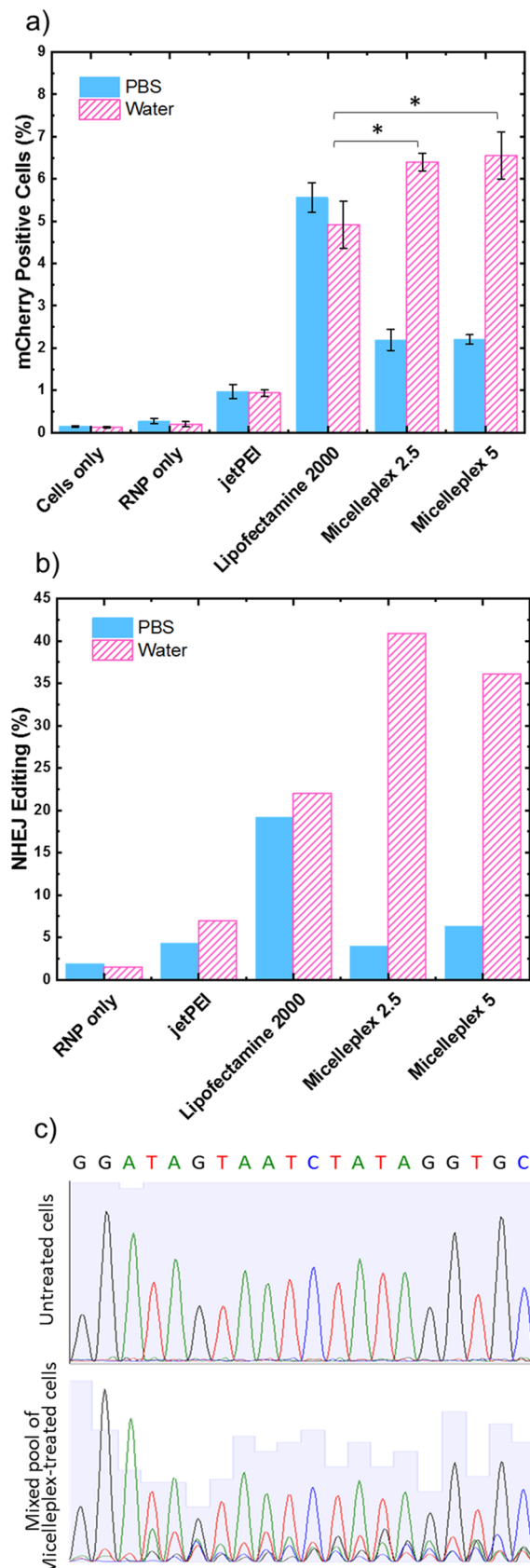


Figure 6. In vitro gene editing achieved by ODB(10) micelleplexes in HEK 293T TLR cells using formulation conditions in PBS and water at polymer:RNP ratios of 2.5:1 and 5:1 along with controls. (a) Percent mCherry⁺ cells measured 48 h post-transfection by flow cytometry. Data presented as mean \pm standard deviation ($n = 3$). The

Figure 6. continued

asterisks “*” indicate statistically different ($p < 0.05$) analyzed by one-way ANOVA followed by a post hoc Tukey test. (b) Percent total NHEJ editing measured by capillary Sanger sequencing and TIDE assay. Data were acquired from the same batch of samples for flow cytometry analysis. Cells from all three wells of the triplicated transfection were combined, and DNA was extracted for sequencing analysis. (c) Representative chromatograms of the sequencing data acquired by transfection with micelleplexes formed in water: 20 bp sgRNA binding region of untreated cells (top) and the cells treated with ODB(10) micelleplexes at polymer:RNP = 2.5:1 (bottom).

6.3%, respectively (Figure 6b, solid blue bars). Although this gene-editing efficiency is moderate, the small, uniform, and well-defined nature of this micelleplex system yields the potential for further optimization for in vivo gene editing. Interestingly, a significant boost in the gene-editing efficiency was achieved by the micelleplex formulations in water. The data showed that slightly over 40% of the cells undergo NHEJ after treatment by the micelleplexes at polymer:RNP 2.5:1, which is significantly higher than that observed with jetPEI and approximately doubled the efficiency of Lipofectamine 2000 (Figure 6b, slashed pink bars). A complete list of the sequencing results is in Table S2, Supporting Information. The sequencing chromatograms of the DNA extracted from cells treated by micelleplexes clearly showed a mixed pool of edited and wild-type cellular DNA (Figure 6c), which is a further indication of the successful and high-efficiency gene editing.

It is intriguing that the micelleplex formation conditions have such a significant impact on micelleplex complexation and gene-editing efficiency. We speculate that the larger micelleplex particle size formed in water is the key to higher in vitro transfection efficiency. Indeed, previous studies with pDNA delivery have shown that solvent ionic strength significantly impacts vehicle-pDNA complex formation, size, and colloidal stability.^{48,49} The previous reports also mentioned that large particle size may play a significant role in accelerating sedimentation of the complexes in cell culture, which promotes a higher concentration of the complexes to interact with the adherent cell monolayer and subsequently increase cellular internalization to promote higher transgene expression.^{48–51} However, this is the first time that this phenomenon has been observed in an RNP delivery system. Quantitative treatment of this theory can be provided by the equation for particle sedimentation velocity (eq 1).⁵⁰ In eq 1, ρ_p is the density of particle, ρ_f and μ_f are fluid density and viscosity, respectively, and g is the gravitational acceleration. With the assumption that micelleplexes formed in water and PBS have similar densities, and the fact that the fluid density and viscosity are the same (as both transfections were completed in culture), the micelleplex sedimentation velocity (ν) is then solely proportional to r^2 , the particle radius. Micelleplexes formed in water have around 5 times larger radii compared to micelleplexes formed in PBS, and thus the sedimentation rate would calculate to be about 25 times higher, which causes a faster accumulation of micelleplexes on the cell surface, presumably increasing cellular uptake and subsequently leading to significantly higher RNP delivery and gene-editing.

$$\nu = \frac{2r^2g(\rho_p - \rho_f)}{\mu_f} \quad (1)$$

Indeed, this work is the first to show the quantitative correlation between formulation conditions and the resultant biological performance, and directly correlate the physico-chemical properties of vehicle-RNP complexes and their genome-editing efficiency. Although large micelleplexes formed in water may be inefficient for in vivo systemic delivery, they could find utility for direct tissue injection. Moreover, their high efficiency could be important and useful for ex vivo or cell therapy-based treatments.

CONCLUSIONS

In this work, four cationic block polymer micelle systems comprising diblock PDMAEMA-*b*-PnBMA and three PEO-*b*-PDMAEMA-*b*-PnBMA triblock variants were prepared and studied as CRISPR/Cas9 ribonucleoprotein delivery vehicles. A high-throughput DLS and high content image cytometry workflow was developed to analyze formulations for hydrodynamic size and gene editing efficiency. This workflow enabled the discovery that ODB(10) revealed statistically higher editing efficiency than the Lipofectamine 2000 positive control. For this reason, the ODB(10) micelleplex system was selected for further quantitative characterization. Well-defined micelleplexes were formed with small and uniform particle sizes in the PBS buffer, and RNPs were shown to bind within the coronas of single micelles, which promoted moderate gene-editing efficiency. Due to the well-defined composition and uniform size, this formulation has the potential to be optimized for in vivo gene editing. In comparison, micelleplexes self-assembled in water formed larger multimicelle particles. It is postulated that the micelles complexed to pre-aggregated RNPs enable faster sedimentation kinetics and thus lead to superior gene-editing efficiency in vitro, twice that of Lipofectamine 2000. This facile packaging method to promote high editing efficacy has the potential to be applied for in vitro and ex vivo gene editing. To the best of our knowledge, this work is the first example of a well-defined polycationic micelle formulation that successfully complexes and delivers CRISPR/Cas9 RNPs, and enabled correlations of the physico-chemical properties, mechanism of packaging, and efficacy of genome editing. Indeed, the novel results presented herein provide future guidance for utilizing cationic polymer micelles and essential characterization techniques to facilitate simple, efficient, and inexpensive gene editing systems for a wide variety of applications.

ASSOCIATED CONTENT

Supporting Information

The Supporting Information is available free of charge on the ACS Publications website at DOI: [10.1021/acs.macromol.9b01645](https://doi.org/10.1021/acs.macromol.9b01645).

Including experimental section, representative high-throughput fluorescence microscopy images, DLS, SLS, additional representative cryo-TEM images, cytotoxicity, representative gating of flow cytometry data, and a complete list of DNA sequencing results ([PDF](#))

AUTHOR INFORMATION

Corresponding Author

*E-mail: treineke@umn.edu.

ORCID ®

Zhe Tan: [0000-0002-3518-0772](https://orcid.org/0000-0002-3518-0772)

Yaming Jiang: [0000-0002-2623-613X](https://orcid.org/0000-0002-2623-613X)

Mitra S. Ganewatta: 0000-0002-9465-8238

Ramya Kumar: 0000-0002-8725-0023

Timothy P. Lodge: 0000-0001-5916-8834

Theresa M. Reineke: 0000-0001-7020-3450

Present Addresses

¹Ingevity Corporation, 5255 Virginia Avenue, North Charleston, SC 29406, United States

[#]DuPont Company, 455 Forest Street, Marlborough, MA 01752, United States

Notes

The authors declare no competing financial interest.

ACKNOWLEDGMENTS

This work was supported partially by the Defense Advanced Research Projects Agency (DARPA) under contract number N660011824041 and the National Science Foundation through the University of Minnesota MRSEC under award number DMR-1420013. Parts of this work was carried out in the Characterization Facility, University of Minnesota, which has received capital equipment funding from the NSF through the UMN MRSEC program under award number DMR-1420013. The image cytometry experiment was done with the assistance of Dr. Guillermo Marques at the University of Minnesota - University Imaging Centers, <http://uic.umn.edu>. We thank Lisa Zeeb for her help with graphic design and generation.

REFERENCES

- (1) Pennisi, E. The CRISPR Craze. *Science* **2013**, *341*, 833–836.
- (2) Doudna, J. A.; Charpentier, E. The New Frontier of Genome Engineering with CRISPR-Cas9. *Science* **2014**, *346*, 1258096.
- (3) Zetsche, B.; Gootenberg, J. S.; Abudayyeh, O. O.; Slaymaker, I. M.; Makarova, K. S.; Essletzbichler, P.; Volz, S. E.; Joung, J.; van der Oost, J.; Regev, A.; Koonin, E. V.; Zhang, F. Cpf1 Is a Single RNA-Guided Endonuclease of a Class 2 CRISPR-Cas System. *Cell* **2015**, *163*, 759–771.
- (4) Strecker, J.; Jones, S.; Koopal, B.; Schmid-Burgk, J.; Zetsche, B.; Gao, L.; Makarova, K. S.; Koonin, E. V.; Zhang, F. Engineering of CRISPR-Cas12b for Human Genome Editing. *Nat. Commun.* **2019**, *10*, 212.
- (5) Komor, A. C.; Kim, Y. B.; Packer, M. S.; Zuris, J. A.; Liu, D. R. Programmable Editing of a Target Base in Genomic DNA without Double-Stranded DNA Cleavage. *Nature* **2016**, *533*, 420–424.
- (6) Wang, L.; Zheng, W.; Liu, S.; Li, B.; Jiang, X. Delivery of CRISPR/Cas9 by Novel Strategies for Gene Therapy. *ChemBioChem* **2019**, *20*, 634–643.
- (7) Wan, T.; Niu, D.; Wu, C.; Xu, F.-J.; Church, G.; Ping, Y. Material Solutions for Delivery of CRISPR/Cas-Based Genome Editing Tools: Current Status and Future Outlook. *Mater. Today* **2019**, *26*, 40–66.
- (8) Kim, S.; Kim, D.; Cho, S. W.; Kim, J.; Kim, J.-S. Highly Efficient RNA-Guided Genome Editing in Human Cells via Delivery of Purified Cas9 Ribonucleoproteins. *Genome Res.* **2014**, *24*, 1012–1019.
- (9) Liu, C.; Zhang, L.; Liu, H.; Cheng, K. Delivery Strategies of the CRISPR-Cas9 Gene-Editing System for Therapeutic Applications. *J. Controlled Release* **2017**, *266*, 17–26.
- (10) Schumann, K.; Lin, S.; Boyer, E.; Simeonov, D. R.; Subramaniam, M.; Gate, R. E.; Haliburton, G. E.; Ye, C. J.; Bluestone, J. A.; Doudna, J. A.; Marson, A. Generation of Knock-in Primary Human T Cells Using Cas9 Ribonucleoproteins. *Proc. Natl. Acad. Sci. U. S. A.* **2015**, *112*, 10437–10442.
- (11) Niu, Y.; Shen, B.; Cui, Y.; Chen, Y.; Wang, J.; Wang, L.; Kang, Y.; Zhao, X.; Si, W.; Li, W.; Xiang, A. P.; Zhou, J.; Guo, X.; Bi, Y.; Si, C.; Hu, B.; Dong, G.; Wang, H.; Zhou, Z.; Li, T.; Tan, T.; Pu, X.; Wang, F.; Ji, S.; Zhou, Q.; Huang, X.; Ji, W.; Sha, J. Generation of Gene-Modified Cynomolgus Monkey via Cas9/RNA-Mediated Gene Targeting in One-Cell Embryos. *Cell* **2014**, *156*, 836–843.
- (12) Chang, N.; Sun, C.; Gao, L.; Zhu, D.; Xu, X.; Zhu, X.; Xiong, J.-W.; Xi, J. J. Genome Editing with RNA-Guided Cas9 Nuclease in Zebrafish Embryos. *Cell Res.* **2013**, *23*, 465.
- (13) Li, L.; Song, L.; Liu, X.; Yang, X.; Li, X.; He, T.; Wang, N.; Yang, S.; Yu, C.; Yin, T.; Wen, Y.; He, Z.; Wei, X.; Su, W.; Wu, Q.; Yao, S.; Gong, C.; Wei, Y. Artificial Virus Delivers CRISPR-Cas9 System for Genome Editing of Cells in Mice. *ACS Nano* **2017**, *11*, 95–111.
- (14) Liu, Y.; Zhao, G.; Xu, C.-F.; Luo, Y.-L.; Lu, Z.-D.; Wang, J. Systemic Delivery of CRISPR/Cas9 with PEG-PLGA Nanoparticles for Chronic Myeloid Leukemia Targeted Therapy. *Biomater. Sci.* **2018**, *6*, 1592–1603.
- (15) Lao, Y.-H.; Li, M.; Gao, M. A.; Shao, D.; Chi, C.-W.; Huang, D.; Chakraborty, S.; Ho, T.-C.; Jiang, W.; Wang, H.-X.; Wang, S.; Leong, K. W. HPV Oncogene Manipulation Using Nonvirally Delivered CRISPR/Cas9 or Natronobacterium Gregoryi Argonaute. *Adv. Sci.* **2018**, *5*, 1700540.
- (16) Luo, Y.-L.; Xu, C.-F.; Li, H.-J.; Cao, Z.-T.; Liu, J.; Wang, J.-L.; Du, X.-J.; Yang, X.-Z.; Gu, Z.; Wang, J. Macrophage-Specific in Vivo Gene Editing Using Cationic Lipid-Assisted Polymeric Nanoparticles. *ACS Nano* **2018**, *12*, 994–1005.
- (17) Timin, A. S.; Muslimov, A. R.; Lepik, K. V.; Epifanovskaya, O. S.; Shakirova, A. I.; Mock, U.; Riecken, K.; Okilova, M. V.; Sergeev, V. S.; Afanasyev, B. V.; Fehse, B.; Sukhorukov, G. B. Efficient Gene Editing via Non-Viral Delivery of CRISPR–Cas9 System Using Polymeric and Hybrid Microcarriers. *Nanomed. Nanotechnol. Biol. Med.* **2018**, *14*, 97–108.
- (18) Zhang, Z.; Wan, T.; Chen, Y.; Chen, Y.; Sun, H.; Cao, T.; Songyang, Z.; Tang, G.; Wu, C.; Ping, Y.; Xu, F.-J.; Huang, J. Cationic Polymer-Mediated CRISPR/Cas9 Plasmid Delivery for Genome Editing. *Macromol. Rapid Commun.* **2019**, *40*, 1800068.
- (19) Fu, Y.; Foden, J. A.; Khayter, C.; Maeder, M. L.; Reyon, D.; Joung, J. K.; Sander, J. D. High-Frequency off-Target Mutagenesis Induced by CRISPR-Cas Nucleases in Human Cells. *Nat. Biotechnol.* **2013**, *31*, 822–826.
- (20) Cradick, T. J.; Fine, E. J.; Antico, C. J.; Bao, G. CRISPR/Cas9 Systems Targeting β -Globin and CCR5 Genes Have Substantial off-Target Activity. *Nucleic Acids Res.* **2013**, *41*, 9584–9592.
- (21) Xu, C.; Lu, Z.; Luo, Y.; Liu, Y.; Cao, Z.; Shen, S.; Li, H.; Liu, J.; Chen, K.; Chen, Z.; Yang, X.; Gu, Z.; Wang, J. Targeting of NLRP3 Inflammasome with Gene Editing for the Amelioration of Inflammatory Diseases. *Nat. Commun.* **2018**, *9*, 4092.
- (22) Chen, Z.; Liu, F.; Chen, Y.; Liu, J.; Wang, X.; Chen, A. T.; Deng, G.; Zhang, H.; Liu, J.; Hong, Z.; Zhou, J. Targeted Delivery of CRISPR/Cas9-Mediated Cancer Gene Therapy via Liposome-Templated Hydrogel Nanoparticles. *Adv. Funct. Mater.* **2017**, *27*, 1703036.
- (23) Zuris, J. A.; Thompson, D. B.; Shu, Y.; Guilinger, J. P.; Bessen, J. L.; Hu, J. H.; Maeder, M. L.; Joung, J. K.; Chen, Z.-Y.; Liu, D. R. Cationic Lipid-Mediated Delivery of Proteins Enables Efficient Protein-Based Genome Editing in Vitro and in Vivo. *Nat. Biotechnol.* **2015**, *33*, 73–80.
- (24) Wang, M.; Zuris, J. A.; Meng, F.; Rees, H.; Sun, S.; Deng, P.; Han, Y.; Gao, X.; Pouli, D.; Wu, Q.; Georgakoudi, I.; Liu, D. R.; Xu, Q. Efficient Delivery of Genome-Editing Proteins Using Bioreducible Lipid Nanoparticles. *Proc. Natl. Acad. Sci. U. S. A.* **2016**, *113*, 2868–2873.
- (25) Mout, R.; Ray, M.; Yesilbag Tonga, G.; Lee, Y.-W.; Tay, T.; Sasaki, K.; Rotello, V. M. Direct Cytosolic Delivery of CRISPR/Cas9-Ribonucleoprotein for Efficient Gene Editing. *ACS Nano* **2017**, *11*, 2452–2458.
- (26) Wang, P.; Zhang, L.; Xie, Y.; Wang, N.; Tang, R.; Zheng, W.; Jiang, X. Genome Editing for Cancer Therapy: Delivery of Cas9 Protein/SgRNA Plasmid via a Gold Nanocluster/Lipid Core-Shell Nanocarrier. *Adv. Sci.* **2017**, *4*, 1700175.
- (27) Hansen-Bruhn, M.; de Avila, B. E.-F.; Beltrán-Gastélum, M.; Zhao, J.; Ramírez-Herrera, D. E.; Angsantikul, P.; Gothelf, K. V.

- Zhang, L.; Wang, J. Active Intracellular Delivery of a Cas9/SgRNA Complex Using Ultrasound-Propelled Nanomotors. *Angew. Chem., Int. Ed.* **2018**, *57*, 2657–2661.
- (28) Ramakrishna, S.; Kwaku Dad, A.-B.; Beloor, J.; Gopalappa, R.; Lee, S.-K.; Kim, H. Gene Disruption by Cell-Penetrating Peptide-Mediated Delivery of Cas9 Protein and Guide RNA. *Genome Res.* **2014**, *24*, 1020–1027.
- (29) Wang, H.-X.; Song, Z.; Lao, Y.-H.; Xu, X.; Gong, J.; Cheng, D.; Chakraborty, S.; Park, J. S.; Li, M.; Huang, D.; Yin, L.; Cheng, J.; Leong, K. W. Nonviral Gene Editing via CRISPR/Cas9 Delivery by Membrane-Disruptive and Endosomolytic Helical Polypeptide. *Proc. Natl. Acad. Sci. U. S. A.* **2018**, *115*, 4903–4908.
- (30) Lostalé-Seijo, I.; Louzao, I.; Juanes, M.; Montenegro, J. Peptide/Cas9 Nanostructures for Ribonucleoprotein Cell Membrane Transport and Gene Edition. *Chem. Sci.* **2017**, *8*, 7923–7931.
- (31) Sun, W.; Ji, W.; Hall, J. M.; Hu, Q.; Wang, C.; Beisel, C. L.; Gu, Z. Self-Assembled DNA Nanoclews for the Efficient Delivery of CRISPR-Cas9 for Genome Editing. *Angew. Chem., Int. Ed.* **2015**, *127*, 12197–12201.
- (32) Yue, H.; Zhou, X.; Cheng, M.; Xing, D. Graphene Oxide-Mediated Cas9/SgRNA Delivery for Efficient Genome Editing. *Nanoscale* **2018**, *10*, 1063–1071.
- (33) Zhou, W.; Cui, H.; Ying, L.; Yu, X.-F. Enhanced Cytosolic Delivery and Release of CRISPR/Cas9 by Black Phosphorus Nanosheets for Genome Editing. *Angew. Chem., Int. Ed.* **2018**, *57*, 10268–10272.
- (34) Alsaiari, S. K.; Patil, S.; Alyami, M.; Alamoudi, K. O.; Aleisa, F. A.; Merzaban, J. S.; Li, M.; Khashab, N. M. Endosomal Escape and Delivery of CRISPR/Cas9 Genome Editing Machinery Enabled by Nanoscale Zeolitic Imidazolate Framework. *J. Am. Chem. Soc.* **2018**, *140*, 143–146.
- (35) Chen, G.; Ma, B.; Wang, Y.; Gong, S. A Universal GSH-Responsive Nanoplatform for the Delivery of DNA, mRNA, and Cas9/SgRNA Ribonucleoprotein. *ACS Appl. Mater. Interfaces* **2018**, *10*, 18515–18523.
- (36) Wang, Y.; Ma, B.; Abdeen, A. A.; Chen, G.; Xie, R.; Saha, K.; Gong, S. Versatile Redox-Responsive Polyplexes for the Delivery of Plasmid DNA, Messenger RNA, and CRISPR-Cas9 Genome-Editing Machinery. *ACS Appl. Mater. Interfaces* **2018**, *10*, 31915–31927.
- (37) Kang, Y. K.; Kwon, K.; Ryu, J. S.; Lee, H. N.; Park, C.; Chung, H. J. Nonviral Genome Editing Based on a Polymer-Derivatized CRISPR Nanocomplex for Targeting Bacterial Pathogens and Antibiotic Resistance. *Bioconjugate Chem.* **2017**, *28*, 957–967.
- (38) Jiang, Y.; Lodge, T. P.; Reineke, T. M. Packaging PDNA by Polymeric ABC Micelles Simultaneously Achieves Colloidal Stability and Structural Control. *J. Am. Chem. Soc.* **2018**, *140*, 11101–11111.
- (39) Won, Y.-Y.; Davis, H. T.; Bates, F. S. Molecular Exchange in PEO-PB Micelles in Water. *Macromolecules* **2003**, *36*, 953–955.
- (40) Choi, S.-H.; Lodge, T. P.; Bates, F. S. Mechanism of Molecular Exchange in Diblock Copolymer Micelles: Hypersensitivity to Core Chain Length. *Phys. Rev. Lett.* **2010**, *104*, No. 047802.
- (41) Sprouse, D.; Jiang, Y.; Laaser, J. E.; Lodge, T. P.; Reineke, T. M. Tuning Cationic Block Copolymer Micelle Size by PH and Ionic Strength. *Biomacromolecules* **2016**, *17*, 2849–2859.
- (42) Laaser, J. E.; Jiang, Y.; Sprouse, D.; Reineke, T. M.; Lodge, T. P. PH- and Ionic-Strength-Induced Contraction of Polybasic Micelles in Buffered Aqueous Solutions. *Macromolecules* **2015**, *48*, 2677–2685.
- (43) Osborn, M. J.; Gabriel, R.; Webber, B. R.; DeFeo, A. P.; McElroy, A. N.; Jarjour, J.; Starker, C. G.; Wagner, J. E.; Joung, J. K.; Voytas, D. F.; von Kalle, C.; Schmidt, M.; Blazar, B. R.; Tolar, J. Fanconi Anemia Gene Editing by the CRISPR/Cas9 System. *Hum. Gene Ther.* **2015**, *26*, 114–126.
- (44) Carlson-Steumer, J.; Abdeen, A. A.; Kohlenberg, L.; Goedland, M.; Molugu, K.; Lou, M.; Saha, K. Assembly of CRISPR Ribonucleoproteins with Biotinylated Oligonucleotides via an RNA Aptamer for Precise Gene Editing. *Nat. Commun.* **2017**, *8*, 1711.
- (45) Laaser, J. E.; Jiang, Y.; Petersen, S. R.; Reineke, T. M.; Lodge, T. P. Interpolyelectrolyte Complexes of Polycationic Micelles and Linear Polyanions: Structural Stability and Temporal Evolution. *J. Phys. Chem. B* **2015**, *119*, 15919–15928.
- (46) Burchard, W. Solution Properties of Branched Macromolecules. In *Branched Polymers II*; Roovers, J., Ed.; Advances in Polymer Science; Springer Berlin Heidelberg: Berlin, Heidelberg, 1999; Vol. 143, pp 113–194, DOI: [10.1007/3-540-49780-3_3](https://doi.org/10.1007/3-540-49780-3_3).
- (47) Brinkman, E. K.; Chen, T.; Amendola, M.; van Steensel, B. Easy Quantitative Assessment of Genome Editing by Sequence Trace Decomposition. *Nucleic Acids Res.* **2014**, *42*, e168–e168.
- (48) Ogris, M.; Steinlein, P.; Kursa, M.; Mechtler, K.; Kircheis, R.; Wagner, E. The Size of DNA/Transferrin-PEI Complexes Is an Important Factor for Gene Expression in Cultured Cells. *Gene Ther.* **1998**, *5*, 1425–1433.
- (49) Wightman, L.; Kircheis, R.; Rössler, V.; Carotta, S.; Ruzicka, R.; Kursa, M.; Wagner, E. Different Behavior of Branched and Linear Polyethylenimine for Gene Delivery in Vitro and in Vivo. *J. Gene Med.* **2001**, *3*, 362–372.
- (50) Luo, D.; Saltzman, W. M. Enhancement of Transfection by Physical Concentration of DNA at the Cell Surface. *Nat. Biotechnol.* **2000**, *18*, 893–895.
- (51) Rinkenauer, A. C.; Schall, A.; Günther, U.; Wagner, M.; Betthausen, E.; Schubert, U. S.; Schacher, F. H. A Paradigm Change: Efficient Transfection of Human Leukemia Cells by Stimuli-Responsive Multicompartment Micelles. *ACS Nano* **2013**, *7*, 9621–9631.